PHYSICAL REVIEW B **81**, 035407 (2010)

Accurate force spectroscopy in tapping mode atomic force microscopy in liquids

Xin Xu, John Melcher, and Arvind Raman
School of Mechanical Engineering and Birck Nanotechnology Center, Purdue University, West Lafayette, Indiana 47907, USA
(Received 17 September 2009; revised manuscript received 9 December 2009; published 7 January 2010)

Existing force spectroscopy methods in tapping mode atomic force microscopy (AFM) such as higher harmonic inversion [M. Stark, R. W. Stark, W. M. Heckl, and R. Guckenberger, Proc. Natl. Acad. Sci. U.S.A. **99**, 8473 (2002)] or scanning probe acceleration microscopy [J. Legleiter, M. Park, B. Cusick, and T. Kowalewski, Proc. Natl. Acad. Sci. U.S.A. **103**, 4813 (2006)] or integral relations [M. Lee and W. Jhe, Phys. Rev. Lett. **97**, 036104 (2006); S. Hu and A. Raman, Nanotechnology **19**, 375704 (2008); H. Hölscher, Appl. Phys. Lett. **89**, 123109 (2006); A. J. Katan, Nanotechnology **20**, 165703 (2009)] require and assume as an observable the tip dynamics in a single eigenmode of the oscillating microcantilever. We demonstrate that this assumption can distort significantly the extracted tip-sample interaction forces when applied to tapping mode AFM with soft cantilevers in liquid environments. This exception is due to the fact that under these conditions the second eigenmode is momentarily excited and the observed tip dynamics clearly contains contributions from the fundamental and second eigenmodes. To alleviate this problem, a simple experimental method is proposed to screen the second eigenmode contributions in the observed tip deflection signal to allow accurate tip-sample force reconstruction in liquids. The method is implemented experimentally to reconstruct interaction forces on polymer, bacteriorhodopsin membrane, and mica samples in buffer solutions.

DOI: 10.1103/PhysRevB.81.035407 PACS number(s): 07.79.Lh

I. INTRODUCTION

Dynamic atomic force microscopy (dAFM), especially amplitude modulated or tapping mode AFM, is now one of the foremost AFM tools used for the nanoscale resolution imaging and compositional contrast with gentle forces of a wide variety of material surfaces under vacuum, ambient or liquid environments. In amplitude modulated AFM (AM AFM) a microcantilever with a sharp tip is driven harmonically near the resonance of a specific eigenmode and brought closer to the sample. As a consequence of the short and long range interactions between the surface atoms on the sample and tip, the tip oscillation amplitude changes to a setpoint amplitude. The setpoint amplitude is held constant by means of a feedback controller that adjusts the height of the cantilever while scanning the sample, thus rendering topography images of the sample.

In AM AFM, the *observables*, that is, those quantities that can be measured directly from the photodetector in an AFM, are the bending and torsion signals. The most important *nonobservable or hidden quantity* in AM AFM is the tip-sample interaction force. The process of relating the observables to the hidden tip-sample interaction forces is called force spectroscopy. In turn, precise knowledge of tip-sample interaction forces allows the identification of local electric charge, van der Waals forces, specific chemical forces, dissipation, elasticity, adhesion, hydrophillicity or hydrophobicity with nanometer resolution on the sample surface, thus realizing dAFM's full potential as an analytical tool. Force spectroscopy in AM AFM can also reveal the peak tip-sample interaction force in a given cycle of oscillation.[1] These peak interaction forces are important to AFM experimentalists because they are the imaging forces exerted to the sample and need to be minimized especially when scanning fragile biological samples. Imaging forces on the order of even a few nanonewtons can irreversibly deform the macromolecule being imaged.

Existing methods for force spectroscopy in AM AFM can be grouped into categories based on their physical implementation: (a) primary harmonic inversion methods that use integral relations involving the amplitude and phase of the primary harmonic as a function of the Z to reconstruct tip-sample interaction forces;[2–5] (b) spectrum inversion (SI) methods which utilize the anharmonic distortions in the deflection wave form at a fixed Z separation to reconstruct tip-sample interaction forces.[6–8] SI methods are particularly attractive since they allow force spectroscopy simultaneously while the cantilever scans the sample. SI methods are also amenable to liquid environments where the anharmonic distortions of the bending signal are large.[7] More recently eccentric tip cantilevers have been proposed as a means to amplify anharmonic distortions in the torsion signal for SI reconstruction.[9] However, this paper focuses on "normal" cantilevers where only the cantilever bending signal is monitored.[2–8] In general, all existing force spectroscopy dAFM methods rely on the ability to quantifiably measure the tip dynamics in a *single eigenmode* of the cantilever.

Recent work on AM AFM has clearly shown that when soft cantilevers (stiffness < 1 N/m) are driven at their fundamental resonance, the second eigenmode is momentarily excited near times of interaction with the sample and the momentarily excited higher eigenmodes are greatly enhanced at low Q factors produced when oscillating under liquids.[10–12] Figure 1 shows a magnetically coated cantilever (MAC lever, Agilent Technologies) tapping on a purple membrane (PM) (bacteriorhodopsin membrane) patch in buffer solution. As shown in this figure, the response of the second eigenmode contributes significant distortions at the bottom of the wave form of the cantilever deflection signals measured at the free end of the cantilever, which, in turn, generates a cluster of enhanced higher harmonics near the second eigenmode natural frequency in the frequency spectrum.[10,11] This phenomenon has been observed to differ-

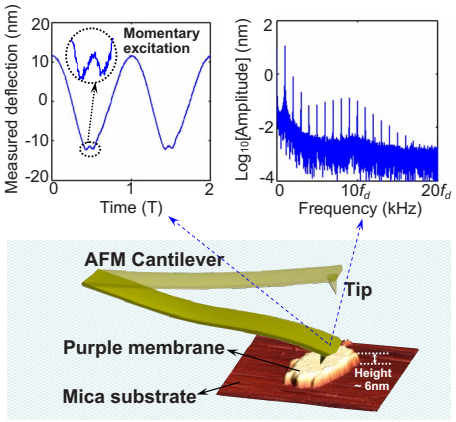

FIG. 1. (Color online) A schematic of a soft MAC lever (Agilent Technologies) tapping on a purple membrane patch in buffer solution (300 mM KCl, 20 mM Tris-HCl). The experimentally measured deflection signals measured at the free end of the cantilever and corresponding spectrum are also plotted. MAC lever properties are listed in Table I, the unconstrained amplitude is 14.1 nm and amplitude setpoint is 83%; the drive frequency is 3.29 kHz.

ent extents for most soft cantilevers (<1 N/m) under most common operation conditions (soft and hard samples, unconstrained amplitude >5 nm, amplitude setpoint range 30–97 %). As a consequence it is increasingly clear that cantilever dynamics in AM AFM in liquids are naturally bimodal without requiring the intentional excitation of the second eigenmode.[13] This in turn brings into question the very validity of prior works on force spectroscopy in AM AFM (Refs. 2–8) when applied to liquid domain dAFM because they assume the measurement of tip dynamics in a single eigenmode of the cantilever.

In this paper, a simple experimental method is proposed that can easily screen the second eigenmode dynamics from the bending signal for the purpose of accurate force spectroscopy in liquids. We begin with introducing the theoretical issue of inverting a signal with contributions from multiple eigenmodes into time-resolved forces. A simple experimental method to screen the contribution of the second eigenmode in the measured bending signal is proposed for the purpose of accurate force spectroscopy in liquids.

II. DYNAMICS OF SOFT CANTILEVERS IN LIQUID

In order to provide a theoretical background to force spectroscopy in liquids, it is necessary to develop a mathematical model for a soft microcantilever tapping on samples in liquid. For simplicity, we will consider only the two-eigenmode model, however it is straightforward to extend the results to the more general N degree-of-freedom (DOF) model. We will also focus on magnetically excited cantilevers since it is easy to interpret their vibration spectrum far from the sample.[14] The two-DOF mathematical model for the magnetically excited, rectangular microcantilever tapping on a sample is[10,15]

$$\frac{\ddot{q}_1}{\omega_1^2} + \frac{\dot{q}_1}{\omega_1 Q_1} + q_1 = \frac{F_{d1}}{k_1}\cos(\omega t) + \frac{F_{ts}(z)}{k_1}, \tag{1a}$$

$$\frac{\ddot{q}_2}{\omega_2^2} + \frac{\dot{q}_2}{\omega_2 Q_2} + q_2 = \frac{F_{d2}}{k_2}\cos(\omega t) + \frac{F_{ts}(z)}{k_2}, \tag{1b}$$

where the subscript $i=1,2$ refers to the first and second eigenmodes, respectively, q_i's are the tip deflections in the ith eigenmode and dots represent temporal derivatives. F_{di}, k_i, Q_i, and ω_i are the equivalent forcing amplitudes, stiffnesses, quality factors, and natural frequencies of the ith eigenmode, respectively, and ω (close to ω_1) is the drive frequency, F_{ts} is the tip-sample interaction force which depends on the instantaneous gap between the tip and the sample $z=Z_c+q_1+q_2$, where Z_c is the separation between the base of the microcantilever and the sample and (q_1+q_2) is the total deflection of the tip. Note these two equations are coupled to each other through the nonlinear tip-sample interaction force F_{ts}. Another important observation is that the tip-sample interaction forces F_{ts} experienced by the first and second eigenmodes are identical.

The above two-DOF model arises from a two-eigenmode Galerkin projection of the original partial differential equation governing the transverse vibrations of a cantilever beam.[10] Accordingly, the forced response of the two-mode cantilever vibration model takes the following form:

$$w(x,t) = q_1(t)\psi_1(x) + q_2(t)\psi_2(x), \tag{2}$$

where $\psi_1(x)$ and $\psi_2(x)$ are the modal shapes of the first and second eigenmodes and are normalized so that $\psi_i(L)=1$ $(i=1,2)$. Furthermore, $q_1(t)$ and $q_2(t)$ are the contributions to the tip displacement of the two flexural modes, respectively, and the tip motion is $w(L,t)=q_1(t)+q_2(t)$. However, most of AFM systems are based on the optical-beam deflection technique and their output signal is proportional to the cantilever slope at the location x^* of the laser spot.[16] For the two eigenmode approximation, the photodiode signal is proportional to $\frac{\partial w(x^*,t)}{\partial x} = q_1(t)\frac{d\psi_1(x^*)}{dx} + q_2\frac{d\psi_2(x^*)}{dx}$. Assuming the photodiode signal is calibrated according to the first eigenmode sensitivity, the calibrated signal becomes

$$u_p(x^*,t) = q_1(t) + \chi(x^*)q_2(t), \tag{3}$$

where $\chi(x^*)=\frac{d\psi_1(x^*)}{dx}/\frac{d\psi_2(x^*)}{dx}$. Note Eq. (3) ignores the finite bandwidth of the photodiode measurement as well as any nonlinearities in the measurement.[17] Typically, the laser spot is focused near the free end of the cantilever $(x^*=L)$. For a rectangular cantilever, standard beam theory predicts $\chi(L)=3.47$. Thus, $u_p(L,t)$ amplifies the motion of the second eigenmode.

Numerical simulations of Eq. (1) are performed for the parameters listed in Table I. Tip-sample interactions are modeled by the Hertz contact model:[18] $F_{ts}(z)=\frac{4}{3}E^*\sqrt{R}(-z)^{3/2}$ for $z\leq 0$ and otherwise zero, where R is the tip radius, E^* is the effective elastic modulus of the tip/sample system and $E^*=[(1-\nu_t^2)/E_t+(1-\nu_s^2)/E_s]^{-1}$, where ν_t, E_t, ν_s, and E_s are the Poisson's ratio and elastic modulus of the tip and sample, respectively. In this simulation we use $E_s=0.45$ GPa, $\nu_s=0.3$.

First, we demonstrate in numerical simulations, the phenomenon of momentary excitation of the second eigenmode in Fig. 2. Figure 2(a) shows the simulated, photodiode signal

TABLE I. Properties of MAC lever in liquid.

$L\times b\times h$ (μm^3)	$350\times 35\times 1.5$
Stiffness (N/m)	0.11
Tip radius (nm)	50
First mode resonance frequency (kHz)	3.93
First mode Q factor	1.85
Second mode resonance frequency (kHz)	30.00
Second mode Q factor	4.29
Elastic modulus (GPa)	169
Poisson's ratio	0.3

$u_p(L,t)$ (for a laser spot located at the free end), which reveals distinct, short time-scale distortions near times of tip-sample contact. The spectrum of $u_p(L,t)$ [Fig. 2(b)] reveals a cluster of peaks centered at the frequency of the second eigenmode. Figure 2(c) shows the modal components $q_1(t)$ and $q_2(t)$ of the photodiode signal. With each tip-sample interaction, q_2 is momentarily excited and rings down. The extent to the ringing of q_2 becomes amplified in $u_p(L,t)$, contributing ripple distortions to the wave form. Furthermore, the periodic momentary excitation of q_2 has a distinct signature in the frequency domain, which is a cluster of peaks centered at the frequency of the second eigenmode [Fig. 2(d)]. Finally, note that several harmonics of $q_1(t)$ and $q_2(t)$ are overlapping in Fig. 2(d). Consequently, it is not possible to separate the deflections $q_1(t)$ and $q_2(t)$ in the observable $u_p(L,t)$ in either frequency domain or time domain.

III. THEORETICAL CONSIDERATIONS FOR FORCE SPECTROSCOPY WITH DUAL EIGENMODE INTERACTIONS

In this section, we discuss the issue of SI force spectroscopy applied to signals containing contributions from two different eigenmodes, as is often the case in liquid domain dAFM. Accurate force spectroscopy is a two-part process. First, unconstrained vibrations are used to calculate the excitation force. Second, the vibration spectra while tapping is used to calculate the total force applied to the cantilever, from which, the excitation force is subtracted to yield the tip-sample interaction force. However, the photodiode signal from the free end $u_p(L,t)=q_1(t)+3.47q_2(t)$ contains a contribution from the second eigenmode. To invert this signal to time-resolved forces is a complicated process that requires knowledge of lumped parameters of the second eigenmode (k_2,ω_2,Q_2) (Ref. 19) as well as, knowledge of the eigenmodes themselves and the excitation force distribution. On the other hand, if the second eigenmode can be screened from the photodiode signal, the force inversion process becomes much simpler, requiring only the lumped parameters of the first eigenmode to be calibrated. In this section, we propose a method by which the second eigenmode dynamics are screened from the photodiode signal in order to achieve accurate tip-sample force measurements.

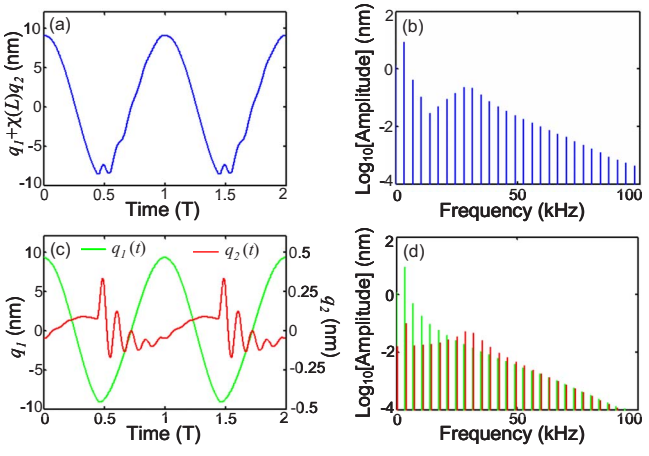

FIG. 2. (Color online) Simulated photodiode wave form and spectra. (a) Simulated photodiode signal measured at the free end $u_p(L,t)=q_1(t)+\chi(L)q_2(t)$, and corresponding amplitude spectrum; (c) simulated modal deflections $q_1(t)$ and $q_2(t)$, and (d) their corresponding amplitude spectra. MAC lever properties are listed in Table I, the unconstrained amplitude is 10.2 nm and amplitude setpoint is 85%; the sample is PTFE (E_s=0.45 GPa, ν_s=0.3).

The proposed method for accurate force spectroscopy in liquid environments is to screen the second eigenmode response from the photodiode signal $u_p(x^*,t)=q_1(t)+\chi(x^*)q_2(t)$. The second eigenmode is screened from the signal when $\chi(x^*)=\frac{d\psi_2(x^*)}{dx}/\frac{d\psi_1(x^*)}{dx}=0$. This occurs when the laser spot is aligned with the antinode of the second eigenmode x^{AN}, which is defined by $\frac{d\psi_2(x^{AN})}{dx}=0$. The tip-sample interaction force is assumed to be a Dirac-delta function at the free end, which makes the total equivalent modal force $F_1(t)=F_{d1}+F_{ts}$. Accordingly, the photodiode signal $u_p(x^{AN},t)$ can be inverted to obtain the tip-sample interaction forces by

$$F_{ts}(j\omega)=-F_{d1}(j\omega)+G^{-1}(x^{AN},j\omega)U_p(x^{AN},j\omega), \qquad (4)$$

where

$$G(x^{AN},j\omega)=\frac{U_p(x^{AN},j\omega)}{F_1(j\omega)}=\frac{1}{k_1}\left[1-\left(\frac{\omega}{\omega_1}\right)^2+\frac{j\omega}{\omega_1 Q_1}\right]^{-1} \qquad (5)$$

is the transfer function. $F_{ts}(t)=f^{-1}\{F_{ts}(j\omega)\}$ is obtained from the inverse Fourier transform. The excitation term $F_{d1}(t)$ can be determined from the response far from the sample (in the absence of interaction forces) and is assumed to be invariant.

Experimentally, the issue with Eq. (4) is that $G^{-1}(x^{AN},j\omega)$ is large in magnitude at high frequencies, causing high-frequency noise to be amplified greatly in the reconstructed force. One solution to the problem of high-frequency noise is possible under the assumption of periodic oscillations. Assuming a period $T=2\pi/\omega_d$, consider an N harmonic approximation of the signal $u_p(x^{AN},t)\approx\langle u_p(x^{AN},t)\rangle+\Sigma_{n=1}^{N}A_n\cos(n\omega_d t-\phi_n)$, where $\langle u_p(x^{AN},t)\rangle$ is the mean deflection, and A_n and ϕ_n are the amplitudes and phase lags, respectively, of the nth harmonic and N is the largest harmonic above the noise floor.[7] Accordingly, Eq. (4) can be approximated as

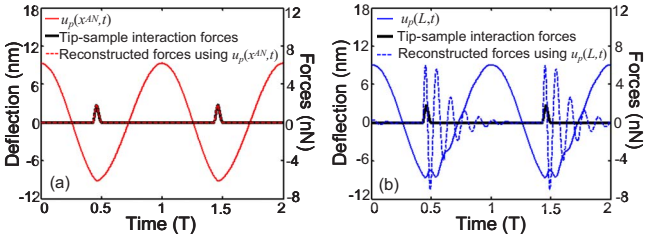

FIG. 3. (Color online) Numerical simulations of tip-sample interaction forces reconstructed by (a) $u_p(x^{AN},t)$ and (b) $u_p(L,t)$. MAC lever properties are listed in Table I; free amplitude is 10.2 nm and amplitude setpoint is 85%; sample is PTFE (E_s =0.45 GPa, ν_s=0.3).

$$F_{ts}(t) \approx -F_{d1}(t) + k_1\langle u_p(x^{AN},t)\rangle + \sum_{n=1}^{N} |G^{-1}(x^{AN},j\omega_n)|A_n \cos(n\omega_d t - \phi_n + \theta_n), \quad (6)$$

where $\tan\theta_n = \frac{n\omega_d\omega_1}{Q_1(n^2\omega_d^2-\omega_1^2)}$. Furthermore, from the unconstrained response (far from the sample), the excitation force is simply $F_{d1}(t)=|G^{-1}(x^{AN},\omega_d)|A_0\cos(\omega_d t-\phi_0+\theta_1)$, where A_0 and ϕ_0 are the unconstrained amplitudes and phase lags, respectively.

Equation (6) is essentially the method described by Stark *et al.*,[6] however, we have assumed that the signal is periodic and used a truncated Fourier series estimation of $u_p(x^{AN},t)$ in place of the full spectrum. The approximations $G^{-1}(x^{AN},j\omega)\approx k_1\omega^2/\omega_1^2$ and $\tan\theta_n\approx 0$ transform Eq. (6) into the scanning probe acceleration microscopy method.[7] However, these approximations are unnecessary. Rather, it is preferred to keep the full form of Eq. (4).

In summary, the second eigenmode response can be easily screened from the photodiode measurement by focusing the detecting laser at the antinode of the second eigenmode and we propose a method to accurately reconstruct the tip-sample interaction forces using the first eigenmode response $[u_p(x^{AN},t)]$ only.

IV. FORCE SPECTROSCOPY IN LIQUIDS: NUMERICAL SIMULATIONS

Now we verify the force reconstruction method that we proposed in last section using $u_p(x^{AN},t)$ by numerical simulations and compare it with the "normal" reconstruction method using $u_p(L,t)$. We reconstruct the tip-sample interaction forces using Eq. (4) from numerical simulations of a MAC lever tapping on polytetrafluoroethylene (PTFE) sample for the parameter values listed in Table I. The reconstructed forces using the first 100 harmonics of the signal $u_p(x^{AN},t)$ [$=q_1(t)$, the first eigenmode motion only] are nearly identical to the actual tip-sample interaction forces [see Fig. 3(a)]. By contrast, the reconstructed forces from the signal $u_p(L,t)$ [$=q_1(t)+3.47q_2(t)$, a combination of first and second eigenmode motion], is quite different from the actual tip-sample interaction force [see Fig. 3(b)]. In fact, the $u_p(L,t)$ reconstruction resembles the response of the second eigenmode, which appear to ring, when the actual forces are just a periodic pulse. Clearly, in this case, the standard photodiode signal at the free end $u_p(L,t)$ cannot be used to accurately reconstruct the tip-sample interaction forces.

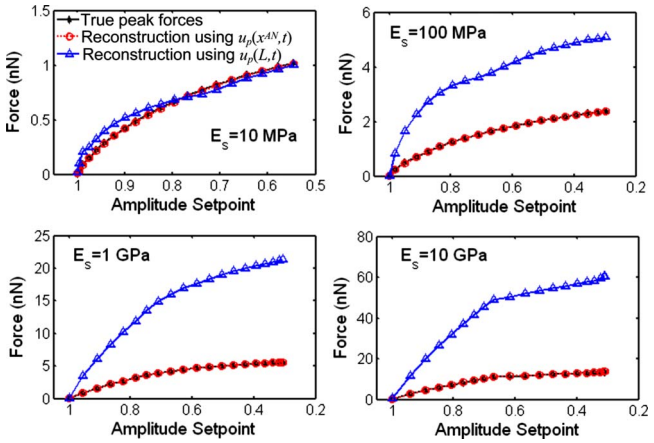

FIG. 4. (Color online) Actual peak tip-sample forces compared with the forces reconstructed from numerical simulations using $u_p(x^{AN},t)$ and $u_p(L,t)$ for different elastic moduli of sample. MAC lever properties are listed in Table I, unconstrained amplitude is 10 nm and driving frequency is 3.5 kHz.

One might ask if there are conditions where the reconstruction from the signal $u_p(L,t)$ can provide a good approximation of $F_{ts}(t)$? As shown in Ref. 11, the momentary excitation of q_2 is less for soft samples. With the MAC lever described in Table I, we simulate the tip-sample interaction forces and their reconstructions using $u_p(L,t)$ and $u_p(x^{AN},t)$ for samples of different stiffnesses. In the simulations the Hertz contact model is used for the tip-sample interaction with sample elastic modulus 10 MPa, 100 MPa, 1 GPa and 10 GPa, respectively. The initial amplitude is set to be 10 nm and the driving frequency is 3.5 kHz. In Fig. 4, the peak repulsive forces are shown vs setpoint. The forces reconstructed from $u_p(x^{AN},t)$ match very well with the actual tip-sample interaction forces $F_{ts}(t)$ in all cases, while the forces reconstructed from $u_p(L,t)$ only match approximately with $F_{ts}(t)$ for very soft samples ($E_s\sim<10$ MPa) where the momentary excitation of higher eigenmodes is very small. Thus, under certain experimental conditions, forces reconstructed from $u_p(L,t)$ may be valid.[8]

V. SCREENING THE SECOND EIGENMODE DYNAMICS: EXPERIMENTS

As we discussed, a simple way to screen the second eigenmode dynamics in experimental measurements is to focus the detecting laser at the antinode of the second eigenmode x^{AN} where the slope of the second eigenmode is 0 [Fig. 5(a)]. Experimentally the location x^{AN} can be located by observing the frequency sweep curve while slowly adjusting the position of the detecting laser along the cantilever length toward the fixed end. This is demonstrated experimentally using the MAC lever (cantilever properties are listed in Table I) in water in Fig. 5(b). When the detecting laser is focused at the free end, the second eigenmode peak is seen around 32 kHz, which is also confirmed by the thermal noise spectrum.

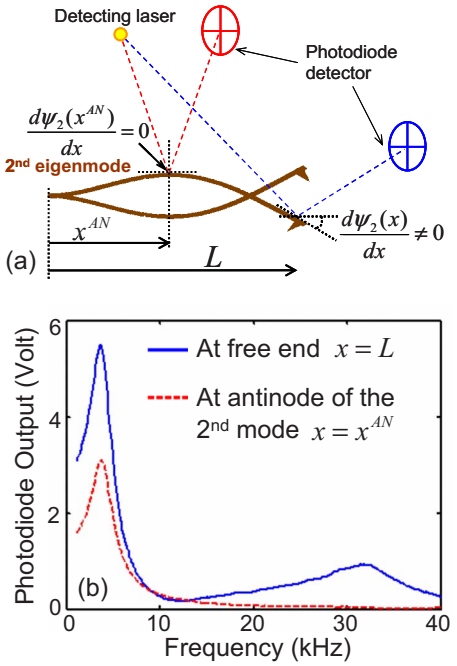

FIG. 5. (Color online) Schematic of photodiode detector position. $x=L$ is the free end of the cantilever; $x=x^{AN}$ is the antinode of the second eigenmode where the slope of the second eigenmode deflection is 0, i.e., the *measured* second eigenmode deflection by the photodiode detector is 0. (b) Frequency sweep curves taken at the free end of cantilever $x=L$ and at the antinode of the second eigenmode $x=x^{AN}$.

When the detecting laser is moved by fine adjustment of the laser alignment screws, toward the antinode of the second eigenmode, the second eigenmode peak gradually diminishes. When the second eigenmode peak disappears from the frequency sweep, we confirm that the detecting laser is located at x^{AN}.

We first demonstrate this technique on a PTFE sample which has an elastic modulus of 0.4–0.55 GPa.[20] The experiment was performed in buffer solution (300 mM KCl, 20 mM Tris-HCl, pH 7.8). The cantilever properties are given in Table I, and the initial amplitude is 10.2 nm and driving frequency is 3.5 kHz.

Figure 6 shows the wave forms and frequency spectra of the photodiode signals $u_p(x^{AN},t)$ and $u_p(L,t)$ at similar amplitude setpoints.[21] In Fig. 6(a), distinct distortions seen in $u_p(L,t)$ near the bottom of the wave form are due to the momentarily excited second eigenmode near times of tip-sample contact. The frequency spectrum of $u_p(L,t)$ in Fig. 6(b) shows that the higher harmonics of the driving frequency that are close to the second eigenmode frequency have been enhanced. This phenomenon has been described in Ref. 11. By comparison, the signal $u_p(x^{AN},t)$ in Fig. 6(c) contains no ripples and the corresponding frequency spectrum does not contain the enhanced harmonics near the frequency of the second eigenmode.

The results in Fig. 6 show two important experimental observations. First, that the dynamics are bimodal—had the response consisted of a single eigenmode $u_p(L,t)$ and $u_p(x^{AN},t)$ would be identical with the possible exception of different signal-to-noise ratios. Second, the response of the second eigenmode has been effectively screened from the signal $u_p(x^{AN},t)$.

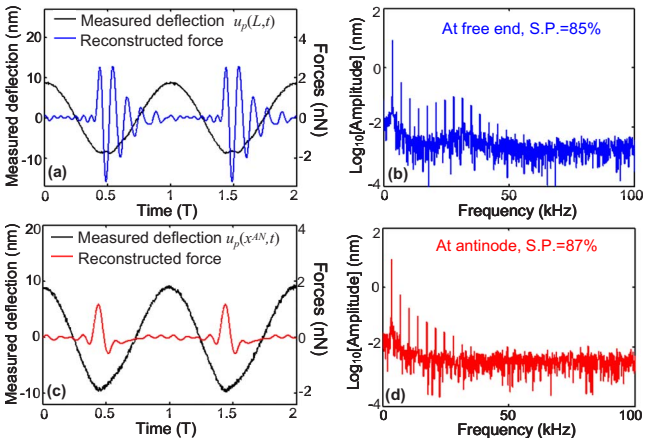

FIG. 6. (Color online) Experimental photodiode signals $u_p(x^*,t)$ and corresponding amplitude spectra measured at the free end ($x^*=L$) and at the antinode of the second mode ($x^*=x^{AN}$) and reconstructed force using $u_p(x^*,t)$. (a) $u_p(L,t)$ and reconstructed force using $u_p(L,t)$; (b) the amplitude spectrum of $u_p(L,t)$; (c) $u_p(x^{AN},t)$ and reconstructed force using $u_p(x^{AN},t)$; (d) the amplitude spectrum of $u_p(x^{AN},t)$. MAC lever properties are listed in Table I; unconstrained amplitude is 10.2 nm; sample is PTFE.

VI. FORCE SPECTROSCOPY IN LIQUIDS: EXPERIMENTS

In this section we demonstrate how the proposed force spectroscopy can be implemented experimentally. The corrected experimental method for accurate force spectroscopy in liquids is achieved by: (1) focusing the detecting laser at the antinode of the second eigenmode by the method described in the previous section. (2) Second, calibrating signal amplitude: our proposed force spectroscopy method requires precise knowledge of $u_p(x^{AN},t)=q_1(t)$, the first eigenmode tip motion. While in the experiments the first eigenmode motion is measured at the antinode of the second eigenmode, whose amplitude is obviously smaller than that of $q_1(t)$ (see Fig. 5). The first eigenmode tip motion can be obtained by scaling the measured antinode motion by a constant coefficient. By assuming that the unconstrained response of the second eigenmode is small compared to the first, this constant coefficient is simply the ratio of the unconstrained tip motion to the unconstrained antinode motion. (3) Finally, reconstructing the tip-sample interaction forces using Eq. (4).

Figure 6(c) also shows the reconstructed forces for a MAC lever tapping on PTFE sample using the above approach. The tip-sample interaction pulse clearly stands out. Note that due to the unavoidable noise in the experimental measurement only finite number of higher harmonics was selected to do the reconstruction. So the reconstructed forces may lose a part of their magnitude. In this case we estimate the lost magnitude is $\sim$10–20 %. For comparison, we also reconstruct forces from the signal $u_p(L,t)$ in Fig. 6(a). Clearly the momentary excitation of the second eigenmode creates serious artifacts in the reconstructed forces.

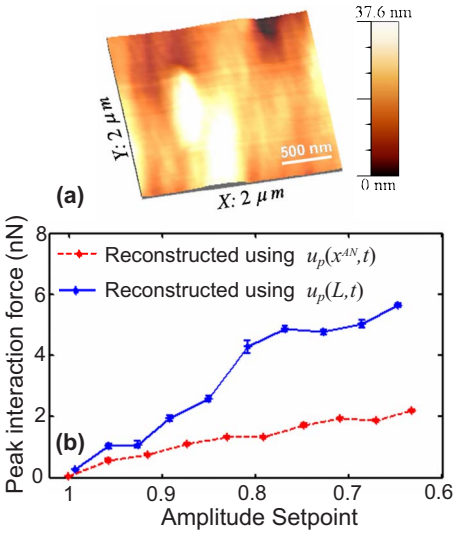

FIG. 7. (Color online) (a) AFM topography image of PTFE sample. (b) Peak tip-sample interaction forces on PTFE reconstructed using $u_p(x^{AN},t)$ (dashed) and $u_p(L,t)$ (solid), respectively, error bars are computed based on five sets of data. MAC lever properties are listed in Table I, unconstrained amplitude is 10.2 nm and driving frequency is 3.5 kHz.

Now we compare the experimental peak tip-sample interaction forces reconstructed from the signals $u_p(x^{AN},t)$ and $u_p(L,t)$ vs amplitude setpoint. We remain with the PTFE sample and the cantilever described in Table I with 10.2 nm free amplitude and 3.5 kHz driving frequency. Figure 7(a) shows the topography image of the PTFE sample. At each amplitude setpoint, we record the photodiode signal for around 50 oscillation cycles. The peak tip-sample forces vs the amplitude setpoint are reconstructed from $u_p(x^{AN},t)$ and $u_p(L,t)$, as seen in Fig. 7(b). The error bars are computed based on five sets of data at each setpoint. The effect of the momentary excitation of second eigenmode, causes the experimental peak tip-sample interaction forces reconstructed from $u_p(L,t)$ to be nearly double of that reconstructed from $u_p(x^{AN},t)$.

VII. APPLICATIONS TO FORCE SPECTROSCOPY ON BIOLOGICAL MEMBRANES SUPPORTED ON STIFF SUBSTRATES

We choose the bacteriorhodopsin membrane (PM, very soft) and mica (very stiff) sample to further explore the implications of present approach. Wild-type purple membrane (Sigma-Aldrich, MO) in distilled water, concentration ~0.5 mg/mL, was diluted by a factor of 10 with 300 mM KCl, 20 mM Tris-HCl (pH 7.8) buffer. 100 μL of the dilute solution was deposit to freshly cleaved mica in a liquid cell. After incubating for 30 minutes, the liquid cell was filled by the same buffer before imaging. At this salt concentration, the elastic modulus of both cytoplasmic (CP) and extracellular (EC) leaflet of the purple membrane is ~15 MPa.[22]

Figure 8(a) shows the AFM topography image of a PM patch deposited on a mica surface in buffer solution. In Fig. 8(b) we compare the experimental peak tip-sample interaction forces on mica and PM reconstructed from $u_p(x^{AN},t)$ and $u_p(L,t)$. We acquire around 280 oscillation cycles of cantilever deflection at each amplitude setpoint. The error bars are based on three sets of data. As expected, the forces reconstructed from $u_p(x^{AN},t)$ and $u_p(L,t)$ give similar results on the very soft PM sample; while on the hard mica surface, the forces reconstructed from $u_p(L,t)$ are nearly double of what obtained by $u_p(x^{AN},t)$, showing the necessity of screening higher eigenmode for accurate force spectroscopy.

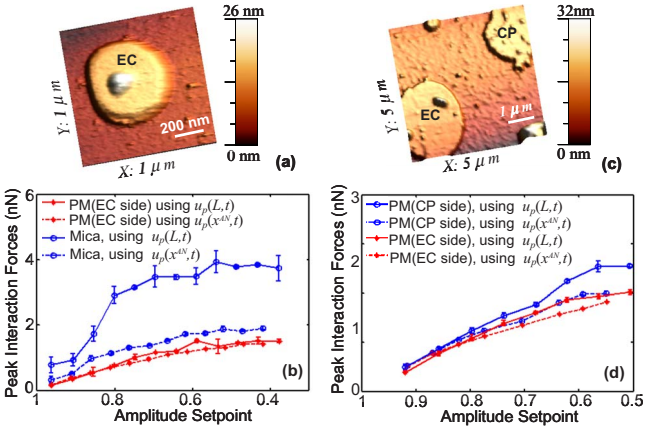

FIG. 8. (Color online) (a) AFM topography image of a PM patch (extracellular leaflet) deposited on mica surface in buffer solution (300 mM KCl, 20 mM Tris-HCl). (b) Experimental peak tip-sample interaction forces on mica and PM as shown in (a) reconstructed using $u_p(x^{AN},t)$(dashed) and $u_p(L,t)$ (solid). MAC lever properties are listed in Table I, unconstrained amplitude is 11.3 nm and driving frequency is 3.5 kHz. (c) AFM topography image of the CP and EC leaflets of PM deposited on mica surface in buffer solution (60 mM KCl, 4 mM Tris-HCl). (d) Experimental peak tip-sample interaction forces on CP and EC leaflets of PM as shown in (c) using $u_p(x^{AN},t)$(dashed) and $u_p(L,t)$ (solid). MAC lever properties are listed in Table I, free amplitude is 10.6 nm and driving frequency is 3.5 kHz.

It is known that the CP and the EC leaflets of purple membrane [see Fig. 8(c) for the topography image of CP and EC leaflet of purple membrane] have different lipid composition and density. For the same sample and cantilever, but with imaging buffer having a lower salt concentration (60 mM KCl, 4 mM Tris-HCl), we repeat the experiment on the two different leaflets. At this salt concentration, the elastic modulus of the CP leaflet is slightly higher than the EC leaflet but both are close to 13 MPa.[22] Again, since both leaflets have a very low elastic modulus, the two reconstructions give similar results, but it is clearly seen that the CP leaflet experiences slightly larger imaging force [Fig. 8(d)] reflecting its slightly larger elastic modulus.

VIII. CONCLUSIONS

For soft microcantilevers tapping in liquids, the momentary excitation of the higher eigenmodes can significantly distort the oscillation wave form recorded by the photodiode rendering inaccurate the existing force spectroscopy methods

in many experimental conditions. By positioning the detecting laser spot at the antinode of the second eigenmode, the first eigenmode dynamics can be easily isolated from the momentary excited second eigenmode dynamics and the first eigenmode motion only has been used to successfully recover the tip-sample forces. Both simulations and experiments prove that the approach proposed in this manuscript works very well in the presence of momentarily excited higher eigenmodes, thus providing an important correction to applications of force spectroscopy in liquids.

ACKNOWLEDGMENT

This research was supported in part by the National Science Foundation under Grants No. CMMI-0700289 and No. CMMI-0927648.

[1] S. Hu and A. Raman, Appl. Phys. Lett. **91**, 123106 (2007).
[2] M. Lee and W. Jhe, Phys. Rev. Lett. **97**, 036104 (2006).
[3] S. Hu and A. Raman, Nanotechnology **19**, 375704 (2008).
[4] H. Hölscher, Appl. Phys. Lett. **89**, 123109 (2006).
[5] A. J. Katan, Nanotechnology **20**, 165703 (2009).
[6] M. Stark, R. W. Stark, W. M. Heckl, and R. Guckenberger, Proc. Natl. Acad. Sci. U.S.A. **99**, 8473 (2002).
[7] J. Legleiter, M. Park, B. Cusick, and T. Kowalewski, Proc. Natl. Acad. Sci. U.S.A. **103**, 4813 (2006).
[8] X. Xu, C. Carrasco, P. J. De Pablo, J. Gomez-Herrero, and A. Raman, Biophys. J. **95**, 2520 (2008).
[9] O. Sahin, Isr. J. Chem. **48**, 55 (2008).
[10] S. Basak and A. Raman, Appl. Phys. Lett. **91**, 064107 (2007).
[11] X. Xu, J. Melcher, S. Basak, R. Reifenberger, and A. Raman, Phys. Rev. Lett. **102**, 060801 (2009).
[12] J. Melcher, C. Carrasco, X. Xu, J. L. Carrascosa, J. Gomez-Herrero, P. J. De Pablo, and A. Raman, Proc. Natl. Acad. Sci. U.S.A. **106**, 13655 (2009).
[13] J. R. Lozano and R. Garcia, Phys. Rev. Lett. **100**, 076102 (2008).
[14] X. Xu and A. Raman, J. Appl. Phys. **102**, 034303 (2007).
[15] A. Raman, J. Melcher, and R. Tung, Nanotoday **3**, 20 (2008).
[16] G. Meyer and N. M. Amer, Appl. Phys. Lett. **56**, 2100 (1990).
[17] S. Crittenden, A. Raman, and R. Reifenberger, Phys. Rev. B **72**, 235422 (2005).
[18] H. Hertz, Journal fur die reine und angewandte Mathematik **92**, 156 (1882).
[19] J. Melcher, S. Hu, and A. Raman, Appl. Phys. Lett. **91**, 053101 (2007).
[20] http://www.mcmaster.com/
[21] Note that due to experimental operation it is difficult to measure the waveforms at exactly the same amplitude setpoint for the free.
[22] K. Voitchovsky, S. A. Contera, M. Kamihira, A. Watts, and J. F. Ryan, Biophys. J. **90**, 2075 (2006).